On the use of DFT+*U* to describe the electronic structure of TiO_2 nanoparticles: $(TiO_2)_{35}$ as a case study

Ángel Morales-García,[a‡] Stephen Rhatigan,[b‡] Michael Nolan, [b*] Francesc Illas [a*]

[a]Departament de Ciència de Materials i Química Física & Institut de Química Teòrica i Computacional (IQTCUB), Universitat de Barcelona. c/ Martí i Franquès 1-11, 08028 Barcelona, Spain

[b]Tyndall National Institute, University College Cork, Lee Maltings, Cork T12 R5CP, Ireland

E-mail: michael.nolan@tyndall.ie, francesc.illas@ub.edu

‡These authors contributed equally

Abstract

One of the main drawbacks in the density functional theory (DFT) formalism is the underestimation of the energy gaps in semiconducting materials. The combination of DFT with an explicit treatment of electronic correlation with a Hubbard-like model, known as DFT+*U* method, has been extensively applied to open up the energy gap in materials. Here, we introduce a systematic study where the selection of *U* parameter is analyzed considering two different basis sets: plane-waves (PWs) and numerical atomic orbitals (NAOs), together with different implementations for including *U*, to investigate the structural and electronic properties of a well-defined bipyramidal $(TiO_2)_{35}$ nanoparticle (NP). This study reveals, as expected, that a certain *U* value can reproduce the experimental value for the energy gap. However, there is a high dependence on the choice of basis set and, and on the +*U* parameter employed. The present study shows that the linear combination of the NAO basis functions, as implemented in FHI-aims, requires a lower *U* value than the simplified rotationally invariant approaches as

implemented in VASP. Therefore, the transferability of *U* values between codes is unfeasible and not recommended, demanding initial benchmark studies for the property of interest as a reference to determine the appropriate value of *U*.

I. INTRODUCTION

Titanium dioxide, TiO_2, nanoparticles involving a mixture of anatase and rutile polymorphs, in particular in the commercialized Degussa P25 form, constitute the most studied photocatalytic material and a model system for the mechanisms involved in photocatalysis.[1-4] The performance of TiO_2 largely depends on its optical, electronic, structural, morphological and surface properties,[5-7] and one of the key properties of TiO_2, especially in the anatase polymorph, is the formation of photogenerated charge carriers (holes and electrons), activated by the absorption of ultraviolet (UV) light. Indeed, the need for UV radiation constitutes one of the major bottlenecks towards developing efficient TiO_2 photocatalysts that can work under sunlight as only ~5% of the incident solar spectrum corresponds to UV light. Hence, a major challenge in the development of competitive TiO_2-based photocatalysts is reducing the energy gap to the visible (VIS) region.[8]

In principle, the properties of TiO_2 can be modulated by designing nanoparticles (NPs) with different sizes, shapes, crystallinities, and surface facets.[9-12]. However, to determine the relationship between structural and electronic properties of TiO_2 nanoparticles, experimentally, is not a simple task. Alternatively, computational techniques provide a feasible, accurate, and unbiased approach to study such correlations and, consequently, can contribute to build connections between experiment and theory.[13]

Density functional theory (DFT)[14,15] has been widely used to study the properties of different types of materials with high accuracy in the prediction of crystal structures and reasonable description of electronic structure features at a moderate computational cost[16] and

with a well-established reproducibility.[17] Unfortunately, energy gaps computed using the popular local density approximation (LDA) and the generalized gradient approximation (GGA) are consistently underestimated by 30–100%[18,19]. The error arises from the inherent lack of derivative discontinuity and the delocalization error.[20-22] To overcome the drawbacks of LDA and GGA for estimating this electronic property, hybrid functionals, which include a part of the nonlocal Fock exchange, have been proposed and widely employed.[18,23,24] Depending on the type of basis set, the use of hybrid functionals can represent a significant increase in the cost of the calculations. Inspired by the Hubbard Hamiltonian,[25] Anisimov et *al.*[26] proposed to avoid the computational load inherent to hybrid functionals by implementing an empirical on-site Hubbard (*U*) correction to a selected atomic energy level, within standard DFT. The resulting method is often referred to as DFT+*U*, an unfortunate term as DFT is an exact theory. DFT+*U* has been broadly used, especially after the contribution of Dudarev *et al.*[27] and is particularly useful in the description of the partially filled *d*-states of the transition metals – in the case of TiO_2, the *U*-correction is applied to the Ti 3*d* orbital.[28,29]

The DFT+*U* method combines the high efficiency of standard DFT with an explicit, albeit approximate and empirical treatment of electron on-site correlation, and constitutes one of the simplest approaches to describe the ground state of strongly correlated systems.[30] However, the choice of the appropriate *U* parameter value for each compound constitutes a challenge. This obstacle can be solved through (*i*) a linear response, fully consistent method,[31] or (*ii*) alternative routes based on comparison with experimental results for some physical property of interest such as magnetic moment, energy gap, redox potentials or reaction enthalpies.[32-34] For instance, the latter strategy has been employed in the study of electron transport in rutile phase,[35,36] of reduced forms of TiO_2,[37,38] and ultrathin films of the rutile phase.[39] Nevertheless, the selection of the *U* parameter is not straightforward. Moreover, the choice of the appropriate form of the projector functions inherent to the method is also a

concern,[40] especially after the work of Kick *et al.*[41] who recently implemented DFT+*U* with a numerical atomic orbital basis set. The authors showed that the value for *U* depends on the choice of projector function, which in turn depends on the type of basis set (atomic orbitals or plane waves) used. The aim of the current study is to evaluate the effect of the basis sets in the selection of the *U* value necessary to describe the electronic structure of semiconducting nanoparticles, taking a previously investigated, well-defined $(TiO_2)_{35}$ bipyramidal NP as a case study.[42]

II. MODELS AND COMPUTATIONAL METHODS

The well-defined bipyramidal stoichiometric $(TiO_2)_{35}$ anatase NP, which fulfills the requirement of a Wulff construction,[43] and was used in previous studies,[42] is selected for the present study (Fig. 1). This nanoparticle exposes the most favorable (101) facets only, as found in experiments.[7] Furthermore, its ~2 nm size is also appropriate to rationalize experimental results reported for TiO_2 anatase NPs.[44]

The calculations reported here have been carried out using two widely used codes, namely the Vienna *Ab Initio* Simulation Package (VASP)[45,46] and the Fritz Haber Institute *ab initio* molecular simulations (FHI-aims).[47] In both cases, the Perdew-Wang (PW91) exchange-correlation functional[48] is used and spin-polarization is accounted for explicitly, although the final results do not exhibit any spin-polarization. The partially filled Ti_{3d} states were consistently described by applying the Hubbard *U* correction[26] under the simplified rotationally invariant approach introduced by Dudarev *et al*.[27] In the following, we will refer to the resulting approach as PW91+*U*, which is more appropriate. The calculations carried out with VASP employ a plane waves (PWs) basis set with a kinetic energy cut-off of 396 eV. To account for the effect of inner electrons on the valence density we implement the projector augmented wave (PAW) method of Bloch[49] as implemented by Kresse and Joubert,[50] with 12 and 6 valence

electrons for Ti and O atoms, respectively. The $(TiO_2)_{35}$ NP is included in a 20 × 20 × 40 Å supercell to give a vacuum gap of 11 Å in the *x*- and *y*-directions and 20 Å in the *z*-direction. Γ-point sampling is used and the convergence criteria for the energy and forces are 10^{-4} eV and 0.02 eV/ $Å^{-2}$, respectively.

On the other hand, the calculations carried out by the FHI-aims code include all electrons (AEs) and account for relativistic effects through the so-called zero-order regular approximation (ZORA)[51,52] proposed earlier by Chang *et al.*[53] A tier-1 light grid numerical atom-centered orbital (NAO) basis set has been used with a quality comparable to that of a TZVP Gaussian Type Orbital basis set for TiO_2.[42] Here, for the implementation of Hubbard *U* correction, the projection functions for Ti_{3d} states are introduced as an explicit linear combination of the NAO basis functions with the double-counting correction in the fully localized limit (FLL); see details in Ref. 41. The convergence threshold for the energy and is 10^{-4} eV. Note that, hereinafter, the notation of PW and NAO is used to refer to the calculations performed with VASP and FHI-aims, respectively.

III. RESULTS AND DISCUSSION

To provide a sound reference for the study, we first discuss the energy gap of fully relaxed anatase and rutile bulk phases as predicted from spin polarized DFT calculations with the PW91 GGA type density functional and using either PW or NAO basis sets. To avoid problems arising from a difference in the quality of the basis sets we increase the kinetic energy cutoff for the PW to 550 eV and used a more extended NAO basis set of tier-2 tight quality. For rutile, the PW/NAO calculated band gap is 1.70/1.91 eV whereas for anatase the PW and NAO calculated band gaps coincide and amount to 2.10 eV. The difference in the rutile phase must be attributed to small differences in the optimized structure arising from the different treatment of the core electrons. In any case, the PW and NAO calculations for bulk rutile and

anatase lead essentially to the same results with a deviation of at most 0.2 eV in the band gap. Clearly, these calculated energy gaps are underestimated with respect to the experimental values, which are 3.0 and 3.2 eV, for rutile and anatase phases, respectively.[54-56] Hybrid functionals with an *ad-hoc* amount of non-local Fock exchange are known to provide a better estimate, as discussed for instance by Ko *et al.*[57], while DFT+*U* can be tuned to recover the experimental band gap, but usually at the cost of a poorer description of other materials properties.

Next we focus on the representative $(TiO_2)_{35}$ anatase NP depicted in Fig. 1. The atomic structure of this NP has been obtained from a geometry optimization using both VASP and FHI-aims computational packages and PW91+*U*. However, to perform a rigorous comparison of the effect of *U* when using PW or NAO basis sets we consider four different situations which are as follows:

(i) The structure is optimized in FHI-aims with PW91 (*U*=0) and single-point calculations are run with both FHI-aims and VASP at each *U* value, *U*=0-10 eV;

(ii) The structure is optimized in VASP with PW91 (*U*=0) and single-point calculations are run with both FHI-aims and VASP at each *U* value, *U*=0-10 eV;

(iii) The structure is fully optimized in both FHI-aims and VASP at each *U*=0-10 eV.

(iv) Each structure obtained by FHI-aims (VASP) in *(iii)* is submitted to a single point calculation in VASP (FHI-aims) at the same *U*-value.

The first and second sets of calculations allow one to investigate differences in the description of the electronic structure that are not due to a difference in the atomic structure but to the different type of basis set and the implementation of the +*U* term.[41] The third set of calculations provides information about differences in the final optimized structure, and the effect of this optimization on the energy gap. Finally, the fourth set of calculations shows to what extent the

fully relaxed atomic structure impacts on the electronic structure. In each of these data sets we can compare the results of the different set-ups by a linear fit of the data.

A. Structure Analysis

We start the discussion by analyzing the structural properties of the $(TiO_2)_{35}$ NP focusing mainly on its length and width (Fig. 2). The PW91 (U=0) fully optimized structures of the $(TiO_2)_{35}$ NP predicted by VASP and FHI-aims are almost the same. In both cases, the nanoparticle length, which is taken from the terminal atoms located in the apical region (see Fig. 1), is 19.61 Å. For the width of the NP, FHI-aims predicts a width that is 0.02 Å larger than VASP. Hence, in the absence of U, both types of basis set lead to the same structure, as expected.[17]

Therefore, any difference in the PW91+U structure predicted by the two types of basis sets (codes) has to be attributed to differences in the implementation of U. Regarding the atomic structure, the main effect of U is to slightly increase nanoparticle length (Fig. 2a). The tendency is consistent, regardless of the basis set, up to U = 5 eV. When U is larger than 5 eV the lengths predicted by VASP and FHI-aims follow different trends. The analysis of the nanoparticle width presents some interesting features (Figs. 2b and 2c). Here the effect of U is different depending on whether the calculation is carried out with a PW or NAO basis set. When using NAO, the optimized NP width drops almost linearly with U up to U = 7 eV, whereas when using PW, the dependence with U is very small, almost negligible. We note that, when using PW, the trends are very stable along the interval of U. However, this is not the case when NAO basis set are employed, and the regular trend is broken at U = 7 eV. Note also that the breaking of the trend at U > 7 eV for the calculations with NAOs indicates that this value is too large to correctly describe correlation effects as it has an exceedingly large influence on the properties of the nanoparticle and induces unreasonable structural changes. Similar observations on the

effect of *U* on the phase stability of TiO_2 have been reported.[33] It is assumed that the large effect of *U* on the atomic structure predicted by the calculations using the NAO basis set arise from the more localized character of the atomic NAO Hubbard projectors as implemented in FHI-aims.[41]

B. Energy Gap Analysis

The analysis of the energy gap of the $(TiO_2)_{35}$ anatase NP provides further interesting comparisons. The Kohn-Sham energy gaps, computed in the set-ups described in scenarios *(i)* and *(ii)*, above, are shown in Fig. 3 and Table I. This data corresponds to two structures, each optimized with the respective codes, FHI-aims and VASP, at the PW91 (U=0) level. We begin by comparing the results of the single-point PW calculations performed on the FHI-aims (green) and VASP (blue) relaxed structures. At each *U*-value, the difference in computed energy gap between the two structures is negligible; in this case, the PW basis set implementation of $+U$ is not sensitive to the geometry at which the electronic structure is computed.

This result contrasts with the NAO data: for each *U*-value, NAO calculations predict a larger energy gap for the FHI-aims structure, relative to the VASP structure. The energy gaps computed from single point NAO calculations over the FHI-aims relaxed structure (red) are positively offset by ~0.5 eV with respect to those values computed over the VASP relaxed structure (black). The change in the energy gap with increasing *U* is consistent, regardless of the atomic structure, as revealed by the slopes (*a*-values) of the red and black trendlines, presented in Table I; i.e. the 0.5 eV offset is maintained over the range of *U*-values. This result is interesting because, as discussed, both FHI-aims and VASP predict similar structures, *vis* length and width, at the PW91 (U=0) level. However, small differences in the atomic structures yield appreciable differences in the energy gaps computed with the NAO basis set, while no

differences were shown with the PW basis set. This highlights that, to avoid misunderstanding interpretations in the analysis of the electronic properties, structural relaxation is crucial when using NAO basis set. It appears that the impact of *U* is greater with NAO, related to the localized projector functions.[41]

It is also interesting to compare NAO and PW results when these calculations are performed on the same starting structure. For the FHI-aims relaxed structure, the energy gaps predicted by NAO (red) and PW (green) calculations are in agreement for small *U*-values, but the differences in the predicted gaps increase with increasing *U*. This is reflected in the slopes (*a*-values) of the trendlines fitted to the NAO (red) and PW (green) data, which are 0.103 and 0.075, respectively (see Table I). In this case, the energy gap varies to a greater extent in the NAO calculations, which consistently predict larger gaps with respect to the PW calculations. Conversely, for the VASP relaxed structure, the energy gaps predicted by NAO (black) and PW (blue) differ over the entire range of considered *U*-values. For $U = 0$ eV, the PW-computed energy gap is larger than that computed with NAO by ~0.5 eV, but this difference decreases with increasing *U*, in accordance with the larger slope for the NAO data (0.106), with respect to that of the PW data (0.080). These results suggest that the differences observed in the computed Kohn-Sham energy gaps are not attributable to differences in the atomic structure, but rather to differences in the implementation of DFT+*U* for the NAO or PW basis set.

Finally, we note that each of the computational set-ups, with the exception of NAO calculations on the VASP relaxed structure (black), predict similar energy gaps of ~2.5 eV for $U = 0$ eV. For these three set-ups, the differences in the computed energy gaps are reasonable, i.e. within 0.15 eV, for *U*-values up to 4 eV. For $U > 4$ eV, the NAO basis set promotes a larger energy gap with respect to the PW basis set.

The data obtained from the calculations described in scenarios *(iii)* and *(iv)*, above, are presented in Fig. 4 and Table II. We first look at the computed energy gaps for the structures

optimized at each *U*-value in FHI-aims (red) and VASP (blue). The energy gaps computed with the NAO basis set increase from 2.5 eV to 3.8 eV as *U* increases from 0 eV to 10 eV. This monotonic increase with *U* is expected and is corroborated in the trendline data, shown in Table II.

Interestingly, the opposite trend is observed for the energy gaps computed for the structures that were fully relaxed at each *U* with the PW basis set: in this case, the energy gaps decrease monotonically with increasing *U*. As seen in our discussion of Figure 3, increasing the *U*-value in a PW calculation on a fixed structure yields a larger energy gap. Thus, here we must attribute the decrease in the energy gaps to effects arising from the structural optimization at each *U*. This result is surprising, not only because it is unexpected, but also because the changes in the PW-computed atomic structures over the range of *U*-values are modest (see Fig. 2), yet the impact on the electronic structure is significant, with states in the gap attributed to the presence of the low coordinated O atoms; see density of states plots in Fig. 5. In fact, for the VASP-relaxed PW91 (*U*=0) structure, a single-point PW calculation with $U = 4$ eV yields an energy gap of 2.76 eV whereas for the fully relaxed structure the energy gap is 2.35 eV. In other words, the emergence of the gap states occurs at lower U values in the PW calculations. This is clearly seen in the density of states plots in Fig. 5 corresponding to the VASP and FHI-aims calculations for $U = 2$ and 6 eV, respectively.

Performing a single-point PW calculation on the FHI-aims relaxed structures at each *U*-value produces the energy gaps represented with the green data points in Figure 4. Here we see that the data points agree with those computed with the NAO basis set (red) within 0.1 eV up to $U = 4$ eV, after which the differences increase. This is in agreement with the trendline data listed in Table II; the slopes for the NAO (red) and PW (green) basis sets are 0.136 and 0.095, respectively. Importantly, single-point PW calculations on the FHI-aims relaxed structures, at each *U*, predict an increase in energy gap with increasing *U*. This further confirms

that the decreasing trend in energy gaps for the VASP-relaxed structures arises from structural effects.

The energy gaps computed with single-point NAO calculations on the VASP-relaxed structures, at each *U*, are shown with the black data points in Fig. 4. An outlier in this data is the energy gap computed for $U = 0$ eV, which is 2.02 eV. This value has been checked and the presence of an error in the calculation can be ruled out. Interestingly, for $U = 1\text{-}10$ eV, the computed energy gaps are consistently ~2.5-2.6 eV and this data shows no discernible increasing or decreasing trend. As seen in our discussion of single-point NAO calculations on both the FHI-aims and VASP PW91 (U=0) relaxed structures, the predicted energy gaps increase monotonically with increasing *U*. Once again, this suggests that subtleties in the structural optimization within the PW implementation of DFT+*U*, probably linked to the low coordinated O atoms at the NP edge, produce these effects in the electronic structure.

For the NAO calculations, consistent with the linear trends for the red data reported in the legends of Figures 3 and 4, the relaxation at each *U* value has a negligible effect, as expected, on the fitting offset with respect to the calculation at the PW91 (U=0) structure. However, the fully relaxed calculations result in changes in the fitting slope. Thus, the opening of the energy gap is more pronounced for the fully optimized structures when employing the NAO basis.

This latter situation, where the NP structure is fully relaxed at each *U* in each code, is the most reasonable scenario to analyze the different behavior observed between basis sets because artifacts due to the use of a structure not optimized within the method/basis set are ruled out. First of all, the energy gaps between the PW and NAO basis set are shifted by 0.25 eV (see Fig. 3), which can be attributed to a different treatment of the effect of the core electrons and also relativistic effects.[58,59] The former are included explicitly in the calculations with the NAO basis set, whereas they are included through a frozen orbital type approach through the

PAW in the calculations with the PW basis. Similarly, the relativistic effects are included explicitly at the ZORA level with the NOA basis and implicitly through the PAW description of the core electrons in the PW calculations. In principle, the most accurate results are obtained from the all-electron basis set implemented in FHI-aims. The most relevant results are found in the variation of the energy gap in response to increasing *U*. These are depicted in Figure 4 and the trends (Table II) reflected in the linear fittings with slopes of 0.136 and -0.028 for NAO and PW basis set, respectively. This result clearly shows the effect of *U* on the resulting energy gap does not only depend on the numerical value of this parameter but also on the projection of the Kohn-Sham states to determine the occupation numbers that enter the +*U* correction and the structural optimization, which, in turn, depend on the basis set used. Thus, the +*U* part of the exchange-correlation potential severely depends on the DFT code, as already shown by Kick *et al.* for some systems.[41]

To clarify this issue, we comment on how results from the PW91+*U* approaches used in the present work can compare to those corresponding to synthetized bipyramidal TiO_2 NPs containing almost 90% of (101) facets that morphologically match quite well with the $(TiO_2)_{35}$ NP model depicted in Fig. 1. UV-Vis diffuse reflectance spectroscopy reported an energy gap of ca. 3.2 eV.[60] To reproduce this result using PW91+*U* requires a *U* value between 4 and 5 eV for the NAO basis set. No *U*-value can reproduce this energy gap for the optimized structures with a PW basis set; however, *U* = 8-9 eV, implemented with a single-point PW calculation on the PW91 (*U*=0) structure does reproduce the experiments. Therefore, the DFT+*U* implementation in FHI-aims entails much lower values of *U* to reproduce results obtained with other codes such as VASP. This is attributed to the strongly localized character of the atomic NAO Hubbard projectors. In short, to achieve a given band gap the value of *U* that is required is much lower with the NAO basis set compared to the plane wave basis set.

In summary, the *U* value fitted to reproduce an experimental or hybrid functional calculated value using a given DFT code cannot be transferred to another code as it depends on the basis set used and, on the method employed to define the corresponding projectors. Thus, for each materials system and DFT code, one should recompute suitable values for *U* through making initial benchmarks.

IV. CONCLUSIONS

The effect of the DFT+*U* method on the structural and electronic properties of the $(TiO_2)_{35}$ NP is systematically investigated by two different basis sets, namely, plane-waves (PWs) and numerical atomic orbitals (NAOs), along with different approaches for the implementation of *U* value. In the absence of *U*, PW and NAO calculations report the same structure and, consequently, the structural variations observed by its inclusion are due to the different implementation of *U* based on a simplified rotationally invariant approach and a linear combination of the NAO basis functions, respectively. Interestingly, the analysis of the energy gap reveals that a certain *U* value can reproduce the experimental value, however, it depends on the basis set and on the employed *U* parameter. Therefore, the transferability of *U* values between codes is not to be recommended and requires initial benchmarks for the property of interest as a reference to find the appropriate value. This study clearly shows that the DFT+*U* implementation in a localized basis set code such as FHI-aims entails much lower values of *U* to reproduce results obtained with a plane wave basis set code such as VASP.

ACKNOWLEDGEMENTS

We thank Matthias Kick for the technical discussion during the elaboration of FHI-aims calculations. The research reported in this work has been supported by the Spanish MICIUN RTI2018-095460-B-I00 and *María de Maeztu* MDM-2017-0767 grants, and, in part, by Generalitat de Catalunya 2017SGR13. A. M.-G. thanks to Spanish MICIUN for a *Juan de la Cierva* postdoctoral grant (IJCI-2017-31979) and F. I. acknowledges additional support from the 2015 ICREA Academia Award for Excellence in University Research. S. R. and M. N. acknowledge support from Science Foundation Ireland through the ERA.Net for Materials Research and Innovation (M-ERA.Net 2), Horizon 2020 grant agreement number 685451, SFI Grant Number SFI/16/M-ERA/3418 (RATOCAT). We acknowledge access to SFI funded computing resources at Tyndall Institute and the SFI/HEA funded Irish Centre for High End Computing (ICHEC). We also acknowledge COST Action CA18234.

TABLE I. Linear fit ($E_{gap} = aU + b$) data for *(i)* optimized $(TiO_2)_{35}$ anatase NP with FHI-aims code at U = 0 eV are calculated by performing single point calculations with FHI-aims code (red) and VASP (green) and *(ii)* optimized structure with VASP code at U = 0 eV by using single point calculations with FHI-aims (black) and VASP (blue) shown in Fig. 3

	Plot Legend		**Trendline**		
	Structure	Single-point	*a*	*b* (eV)	R^2
Red	FHI-aims (*U*=0)	FHI-aims (each *U*)	0.103	2.510	0.989
Green	FHI-aims (*U*=0)	VASP (each *U*)	0.075	2.510	0.999
Black	VASP (*U*=0)	FHI-aims (each *U*)	0.106	1.980	0.984
Blue	VASP (*U*=0)	VASP (each *U*)	0.080	2.450	0.998

TABLE II. Linear fit ($E_{gap} = aU + b$) data for *(iii)* the fully optimized $(TiO_2)_{35}$ anatase NP with the FHI-aims code (red) and VASP code (blue) and *(iv)* single-point calculations in VASP (green) on the FHI-aims relaxed structure for each *U* and single-point calculations in FHI-aims (black) on the VASP-relaxed structure at each *U* shown in Fig. 4.

	Plot Legend		**Trendline**		
	Structure	Single-point	*a*	*b* (eV)	R^2
Red	FHI-aims (each *U*)	-	0.136	2.520	0.993
Green	FHI-aims (each *U*)	VASP (each *U*)	0.095	2.550	0.994
Black	VASP (each *U*)	FHI-aims (each *U*)	0.027	2.310	0.358
Blue	VASP (each *U*)	-	-0.028	2.450	0.994

FIG. 1 Stoichiometric $(TiO_2)_{35}$ anatase NP with bipyramidal morphology. All the exposed facets correspond to the (101) surface. The dimensions of the NP are indicated with double arrows. W_x and W_y denote the nanoparticle width in the *x* and *y* direction, respectively. Gray and red spheres represent Ti and O atoms, respectively.

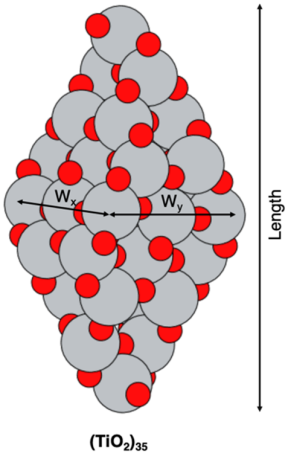

FIG. 2 Evolution of the dimensionality of the stoichiometric $(TiO_2)_{35}$ anatase NP based on (a) length, (b) width in *x* and (c) width in *y* as a function of the *U* parameter for fully optimized structures by using VASP (blue dots) and FHI-aims (red dots) codes.

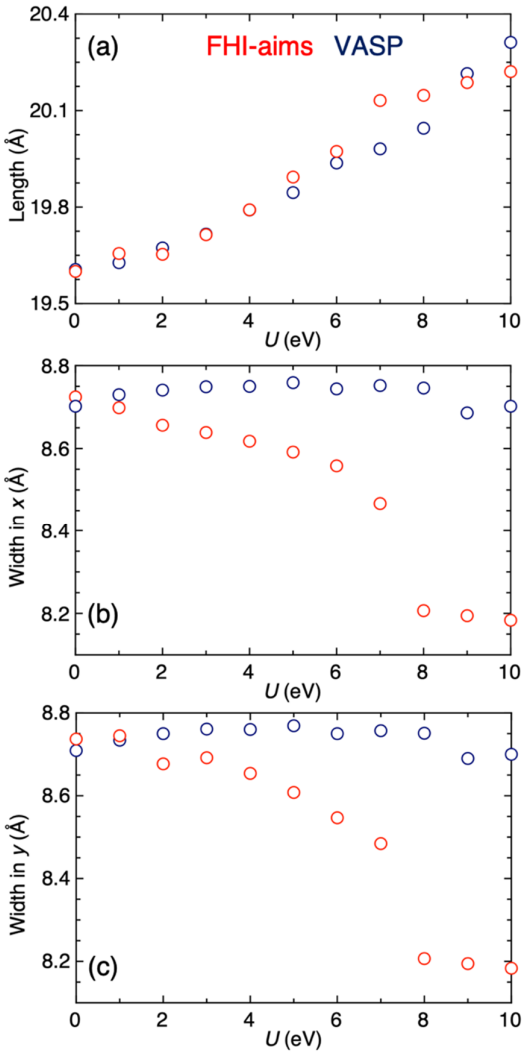

FIG. 3 Variation of the energy gap with the parameter of *U*. The energy gap trends of *(i)* optimized $(TiO_2)_{35}$ anatase NP with FHI-aims code at U = 0 eV are calculated by performing single point calculations with FHI-aims code (red) and VASP (green) and *(ii)* optimized structure with VASP code at U = 0 eV by using single point calculations with FHI-aims (black) and VASP (blue). Details of the linear fit ($E_{gap} = aU + b$) data for each trendline are listed in Table I.

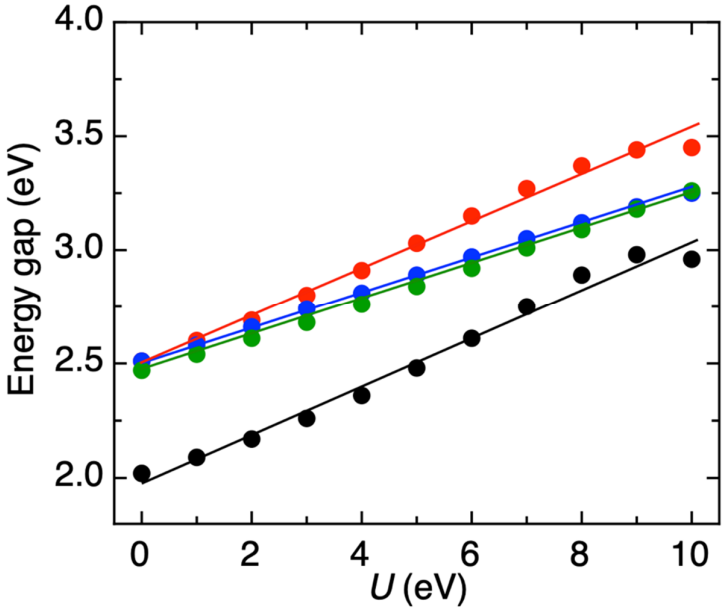

FIG. 4 Variation of the energy gap with the parameter of U for: (scenario *(iii)*) the fully optimized $(TiO_2)_{35}$ anatase NP with the FHI-aims code (red) and VASP code (blue) and (scenario *(iv)*) single-point calculations in VASP (green) on the FHI-aims relaxed structure for each U and single-point calculations in FHI-aims (black) on the VASP-relaxed structure at each U. Details of the linear fit ($E_{gap} = aU + b$) data for each trend-line are listed in Table II.

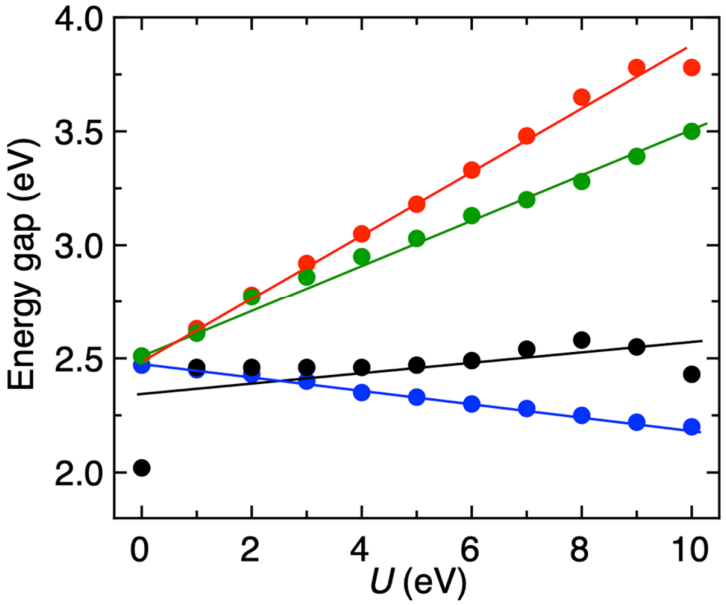

FIG. 5 Projected electronic density of states (PEDOS) of the full relaxed $(TiO_2)_{35}$ NP using PW and NAO basis sets for *U*=0, 2, 4, and 6 eV.

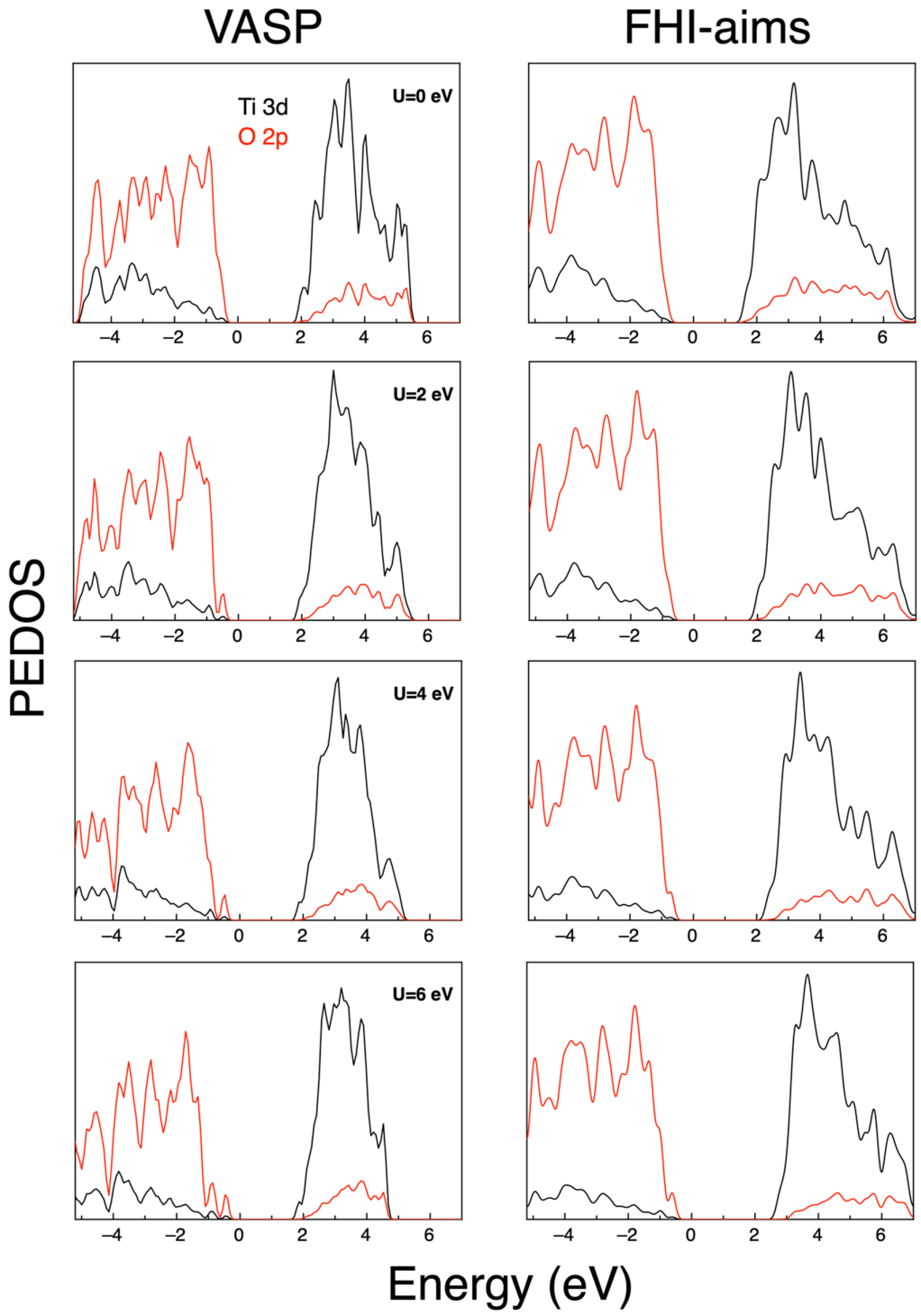

REFERENCES

1 T. Ohno, K. Sarukawa, K. Tokieda and M. Matsumura, J. Catal. **203**, 82 (2001).

2 A. Fujishima, T. N. Rao and D. A. Tryk, J. Photochem. Photobiol. C **1**, 1(2000).

3 A. Fujishima, X. Zhang and D. A. Tryk, Electrochim. Acta **45**, 4683 (2000).

4 K. Hashimoto, H. Irie and A. Fujishima, Jpn. J. Appl. Phys.**44**, 8269 (2005).

5 M. Gao, L. Zhu, W. L. Ong, J. Wang and G. W. Ho, Catal. Sci. Technol.**5**, 4703 (2015).

6 A. Naldoni, M. Altomare, G. Zoppellaro, N. Liu, S. Kment, R. Zboril and P. Schmuki, ACS Catal. **9**, 345 (2019).

7 D. Cho, K. C. Ko, O. Lamiel-García, S. T. Bromley and F. Illas, J. Chem. Theory Comput.**12**, 3751 (2016).

8 X. Chen, L. Liu, P. Y. Yu and S. S. Mao, Science **331**, 746 (2011).

9 X. Chen and S. S. Mao, Chem. Rev.**107**, 2891 (2007).

10 X. Chen, C. Li, M. Graetzel, R. Kostecki and S. S. Mao, Chem. Soc. Rev. **41**, 7909 (2012)

11 D. Selli, G. Fazio and C. Di Valentin, Catalysts **7**, 357 (2017).

12 Á. Morales-García, A. M. Escatllar, F. Illas and S. T. Bromley, Nanoscale **11**, 9032 (2019).

13 E. Clot, Dalton Trans.**43**, 11092 (2014).

14 W. Kohn and L. J. Sham, Phys. Rev.**140**, A1133 (1965).

15 P. Hohenberg, Phys. Rev. **136**, B864 (1964).

16 K. Burke, J. Chem. Phys. **136**, 150901 (2012).

17 K. Lejaeghere, G. Bihlmayer, T. Björkman, P. Blaha, S. Blügel, V. Blum, D. Caliste, I. E. Castelli, S. J. Clark, A. Dal Corso et al. Science **351**, aad3000 (2016).

18 I. de P.R. Moreira, F. Illas and R. L. Martin, Phys. Rev. B **65**, 155102 (2002).

19 C. S. Wang and J. P. Perdew, Phys. Rev. Lett. **51**, 597 (1983).

20 L. J. Sham and M. Schlüter, Phys. Rev. Lett. **51**, 1888 (1983).

21 P. Mori-Sánchez and A. J. Cohen, Phys. Chem. Chem. Phys.**16**, 14378 (2014).

22 P. Mori-Sánchez, A. J. Cohen and W. Yang, Phys. Rev. Lett. **100**, 146401 (2008).

23 J. Muscat, A. Wander and N. M. Harrison, Chem. Phys. Lett. **342**, 397 (2001).

24 A. D. Becke, J. Chem. Phys. **98**, 1372 (1993)

25 J. Hubbard, Proc. R. Soc. London, Ser. A **276**, 238 (1963).

26 V. I. Anisimov, J. Zaanen and O. K. Andersen, Phys. Rev. B **44**, 943 (1991).

27 S. L. Dudarev, G. A. Botton, S. Y. Savrasov, C. J. Humphreys and A. P. Sutton, Phys. Rev. B **57**, 1505 (1998).

28 N. S. Portillo-Vélez, O. Olvera-Neria, I. Hernández-Pérez and A. Rubio-Ponce, Surf. Sci. **616**, 115 (2013).

29 M. T. Curnan and J. R. Kitchin, J. Phys. Chem. C **119**, 21060 (2015).

30 L. Wang, T. Maxich and G. Ceder, Phys. Rev. B **73**, 195107 (2006).

31 M. Cococcioni and S. de Gironcoli, Phys. Rev. B **71**, 035105 (2005).

32 C. Loschen, J. Carrasco, K. M. Neyman and F. Illas, Phys. Rev. B **75**, 035115 (2007).

33 M. E. Arroyo-de Dompablo, Á. Morales-García and M. Taravillo, J. Chem. Phys.**135**, 054503 (2011).

34 Z. Hu and H. Metiu, J. Phys. Chem. C **115**, 5841 (2011).

35 N. A. Deskins and M. Dupuis, Phys. Rev. B **75**, 195212 (2007).

36 C. Persson and A. F. da Silva, Appl. Phys. Lett. **86**, 231912 (2005).

37 E. Finazzi, C. Di Valentin, G. Pacchioni and A. Selloni, J. Chem. Phys.**129**, 154113 (2008).

38 B. J. Morgan and G. W. Watson, J. Phys. Chem. C **114**, 2321 (2010).

39 G. Barcaro, I. O. Thomas and A. Fortunelli, J. Chem. Phys.**132**, 124703 (2010).

40 B. Himmetoglu, A. Floris, S. de Gironcoli and M. Cococcioni, Int. J. Quantum Chem. **114**, 14 (2014).

41 M. Kick, K. Reuter and H. Oberhofer, J. Chem. Theory Comput. **15**, 170 (2019).

42 O. Lamiel-García, K. C. Ko, J. Y. Lee, S. T. Bromley and F. Illas, J. Chem. Theory Comput. **13**, 1785 (2017).

43 G. Wulff, Z. Kristallogr. **34**, 44 (1901).

44 S. Pigeot-Rémy, F. Dufour, A. Herissan, V. Ruaux, F. Maugé, R. Hazime, C. Foronato, C. Guillard, C. Chaneac, O. Durupthy, C. Colbeau-Justin and S. Cassaignon, Appl. Catal. B: Environ. **203**, 324 (2017).

45 G. Kresse and J. Hafner, Phys. Rev. B **49**, 1425 (1994).

46 J. Furthmüller, J. Hafner and G. Kresse, Phys. Rev. B **53**, 7334 (1996).

47 V. Blum, R. Gehrke, F. Hanke, P. Havu, X. Ren, K. Reuter, M. Scheffler and H. Havu, Comput. Phys. Commun. **180**, 2175 (2009).

48 J. P. Perdew, K. Burke and Y. Wang, Phys. Rev. B **54**, 16533 (1996).

49 P. E. Blöchl, Phys. Rev. B **50**, 17953 (1994).

50 G. Kresse and D. Joubert, Phys. Rev. B **59**, 1758 (1999).

51 E. van Lenthe, R. van Leeuwen, E. J. Baerends and J. G. Snijders, Int. J. Quantum Chem. **57**, 281 (1994)

52 M. K. Y. Chan and G. Ceder, Phys. Rev. Lett.**105**, 196403 (2010)

53 C. Chang, M. Pelissier, P. Durand, Phys. Scr. **34**, 394 (1986)

54 A. Amtout and R. Leonelli, Phys. Rev. B **51**, 6842 (1995).

55 S. P. Kowalczyk, F. R. McFeely, L. Ley, V. T. Gritsyna and D. A. Shirley, Solid State Commun. **23**, 161 (1977).

56 D. O. Scanlon, C. W. Dunnill, J. Buckeridge, S. A. Shevlin, A. J. Logsdail, S. M. Woodley, C. R. A. Catlow, M. J. Powell, R. G. Palgrave and I. P. Parkin, Nat. Mater. **12**, 798 (2013).

57 K. C. Ko, O. Lamiel-García, J. Y. Lee and F. Illas, Phys. Chem. Chem. Phys. **18**, 12357 (2016).

58 G. B. Bachelet, N. E. Christensen, Phys. Rev. B **31**, 879 (1985).

59 B. Sadigh, A. Kutepov, A. Landa and P. Söderlind, Appl. Sci. **9**, 5020 (2019).

60 M. D´Arienzo, M. V. Dozzi, M. Redaelli, B. Di Credico, F. Morazzoni, R. Scotti, and S. Polizzi, J. Phys. Chem. C **119**, 12385 (2015).